



Modelling of flow rate in a photovoltaic-driven roof slate-based solar ventilation air preheating system

N. Odeh *, T. Grassie, D. Henderson, T. Muneer

School of Engineering, Napier University, Merchiston Campus, Edinburgh EH10 5DT, UK

Received 7 December 2004; accepted 10 June 2005

Available online 28 July 2005

Abstract

This paper describes the modelling of flow rate in a photovoltaic (PV) driven, roof slate based solar system for preheating ventilation air in cold climates. The system consists of a photovoltaic driven, attic mounted fan, which draws air through the spaces between the warm slates and delivers it through a metallic flexible duct into a house. A model for predicting the flow rate of air as a function of irradiance and ambient temperature is developed based on the measured performance of the different components of the system. Considering all experimental sources of error, the model predicts the flow rate of air with a maximum error of 12%. The model is validated for different combinations of components in a roof section constructed at Napier University in Edinburgh. The predicted flow rates are within 10% of the measured values. The model is extended so that it can be applied for different locations and different roof tilts and orientations. A future paper will make use of the model developed herein for system optimisation based on maximum monthly volume of preheated ventilation air delivered. The model will also be used to investigate the effectiveness of PV driven, roof slate based systems as solar air heaters.

© 2005 Elsevier Ltd. All rights reserved.

Keywords: Condensation dampness; Fan characteristics; Flow rate modelling; Photovoltaic; Roof slates; Ventilation

* Corresponding author. Tel.: +44 131 455 2271; fax: +44 131 455 2264.
E-mail address: n.odeh@napier.ac.uk (N. Odeh).

1. Introduction

Condensation dampness and mould growth are common features of modern living and more energy efficient homes. All houses and apartments require an efficient way to remove moist indoor air, which causes mould formation and, consequently, health problems such as the sick building syndrome (SBS) [1]. Removal of moist and stale air by ventilation makes a house healthier for the occupants and protects the building structure from damage. Several researchers have studied the enhancement of the rate of negative pressure natural ventilation (NPNV) of buildings using solar chimneys and solar air heaters [2,3]. Khedari et al. [4], on the other hand, implemented a small PV driven fan in the structure of a roof solar collector (RSC) to increase the NPNV rates. Natural ventilation, however, depends on wind speed and, depending on the outdoor temperature, can result in high heating bills and uncomfortable draughts in the winter. A positive pressure mechanical ventilation (PPMV) system can provide consistent ventilation through all seasons of the year [5,6].

Standard roof tiles can be many degrees warmer than the ambient outside air [7]. A PPMV system can be designed both to ventilate the house underneath and to harness this extra heat and supply it to the house by means of a small fan [8]. This supplied heat can contribute to the heating demand, thus reducing the need for auxiliary heating as well as reducing heating bills. Generally, a mechanical ventilation system has the disadvantage of requiring an auxiliary electric source to operate the fan [9]. This drawback of the system can be overcome by using a photovoltaic (PV) module, which can also act as a fast response sensor, to power the fan [10].

2. System description

A sketch of the roof slate based (RSB) solar ventilation air preheater under study is shown in Fig. 1. A PV driven axial flow fan, situated in a well sealed wooden box between the joists in the roof, draws air through the spaces between the slates and through holes in the sarking board before delivering it into a flexible duct extended across the attic from the fan box to the room ceiling. In addition to having the advantage of being easily mountable with ducts, axial flow fans are appropriate for low pressure high flow rate applications [11]. As air is drawn past the hot slates, it absorbs the energy stored before being delivered through the flexible duct into the house.

The slates can be treated as a flat plate roof solar collector. Thermal efficiency calculations require a careful definition of the roof area from which heat is extracted and also a study of the air flow patterns underneath the slates. These considerations are beyond the scope of this paper. The current paper is concerned with predicting the flow rate of air delivered to the house as a function of irradiance and ambient temperature in addition to other factors such as the PV module, the fan and the duct specifications. Modelling of the flow rate contributes to the future goal of estimating the thermal contribution of RSB solar ventilation air preheating systems.

Most available literature on flow rate modelling of PV driven systems is on water pumping and solar water heating applications. Jafar [12] gave empirical relationships of flow rate as a function of irradiance at different pumping heads. The coefficients of these quadratic relationships were expressed as functions of head. Bione et al. [13] also showed a quadratic relationship between flow rate and irradiance in a PV driven water pumping system. In other cases, the flow rate of water

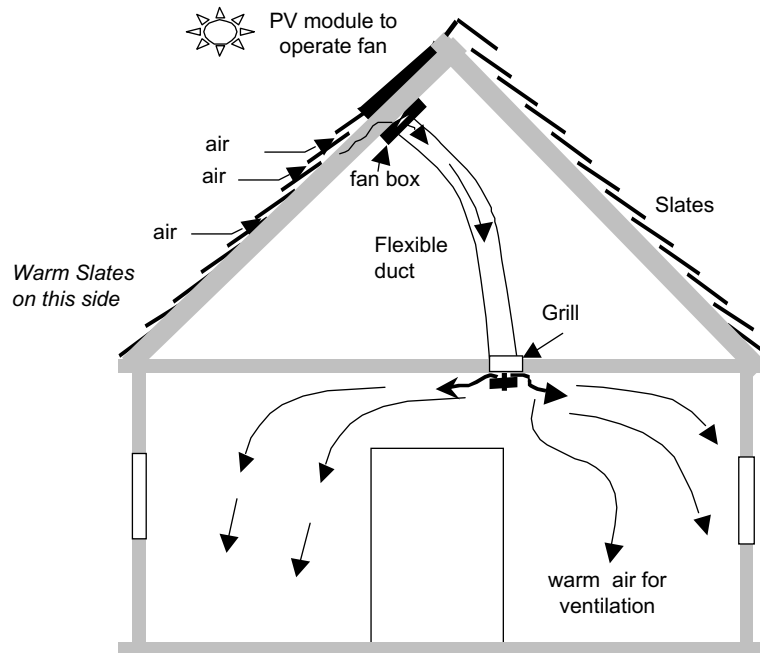


Fig. 1. A sketch of the PV driven RSB solar ventilation air preheating system under study.

was expressed as a quadratic function of the pump voltage [14]. These approaches, as they do not account for the different variables associated with the piping system, are specific, thus limiting their range of application.

Other researchers, on the other hand, through considering the properties of the piping system in their models, have broadened their range of applications. Betka and Moussi [15] and Eckstein et al. [16] described the pump pressure as a function of flow rate and fan rotational speed, which is, in turn, a function of irradiance. The system pressure was expressed as the sum of the static head and friction head. Benlarbi et al. [17] gave the pressure losses in terms of pipe length, diameter and a coefficient representing regular losses. The flow rate in the system is then determined by simultaneously solving the pressure–flow equation for system losses with that for losses across the pump.

The following section describes the mathematical model for the RSB system under investigation. The flow rate of air is expressed as a function of several parameters including irradiance (G , W/m^2), ambient temperature (T_{amb} , $^{\circ}\text{C}$), fan electrical and pressure–flow (ΔP – Q) characteristics and the properties of the flexible duct (i.e. length (L , m), diameter (D , m) and degree of extension (Ext., %)). The model developed is based on measurements and is validated through comparison of the predicted flow rates with the measured values over a range of operating conditions for different systems.

A sub-model is given for each of the three major components of the flow system: the PV module, the fan and the duct. Moreover, the effect of the “slate packing” (i.e. how packed and resistant to flow the slates are) on the fan characteristics is investigated. The development of the three sub-models is based on typical experimental measurements, which serve as reference conditions.

Sections 3.1–3.3 introduce these sub-models, and give descriptions of the experimental procedures and results associated with their development.

3. Mathematical model for PV driven RSB systems

3.1. Photovoltaic model

The electrical output of the PV module is described by its I – V characteristic. This characteristic changes as a function of incident irradiance (G , W/m^2) and PV module temperature (T_{mod} , $^{\circ}\text{C}$) and can be simplified by Eq. (1) as follows:

$$I = I_{\text{sc}} - I_0 \left(e^{\frac{V+I R_s}{A}} - 1 \right) \quad (1)$$

The adaptation of Eq. (1) to define module output as a function of irradiance and module temperature is presented by the SANDSTROM model [18]. It can be described by the following equations:

$$V = V_{\text{ref}} + \mu_{V_{\text{oc}}} \cdot (T_{\text{mod}} - T_{\text{mod,ref}}) - R_s \cdot \Delta I \quad (2)$$

$$I = I_{\text{ref}} + \Delta I \quad (3)$$

where

$$\Delta I = \mu_{I_{\text{sc}}} \cdot \left(\frac{G}{G_{\text{ref}}} \right) \cdot (T_{\text{mod}} - T_{\text{mod,ref}}) + \left(\frac{G - G_{\text{ref}}}{G_{\text{ref}}} \right) \cdot I_{\text{sc}} \quad (4)$$

where V (V) and I (A) are, respectively, the voltage and its corresponding current on the I – V curve at the desired values of G and T_{mod} , I_{sc} is the short circuit current (A), the subscript “ref” represents measurements at reference conditions (i.e. G_{ref} and $T_{\text{mod,ref}}$) and $\mu_{V_{\text{oc}}}$ ($\text{V}/^{\circ}\text{C}$) and $\mu_{I_{\text{sc}}}$ ($\text{A}/^{\circ}\text{C}$) are, respectively, the open circuit voltage and short circuit current temperature coefficients. The series resistance R_s is assumed constant. The equations above also assume that the voltage and current temperature coefficients are constant and equal to $\mu_{V_{\text{oc}}}$ and $\mu_{I_{\text{sc}}}$, respectively. The module temperature T_{mod} can be related to ambient temperature using the following equation:

$$T_{\text{mod}} = T_{\text{amb}} + \frac{G}{800} (\text{NOCT} - 20) \quad (5)$$

where NOCT is the nominal operating cell temperature ($^{\circ}\text{C}$). Fig. 2 shows a comparison of predicted and measured performance data.

3.2. Fan characteristics modelling

3.2.1. Voltage, current and fan rotational speed relationships

The fan’s current–voltage (I – V) and speed–voltage (ω – V) characteristics are both linear of the form $y = C \cdot x$ where C is the slope of the best fit line. The slopes of each of the characteristics for two tested fans, Fan1 and Fan2 are shown in Table 1. The characteristics for Fan1 and Fan2 were determined experimentally by varying the voltage from a power pack while readings of current

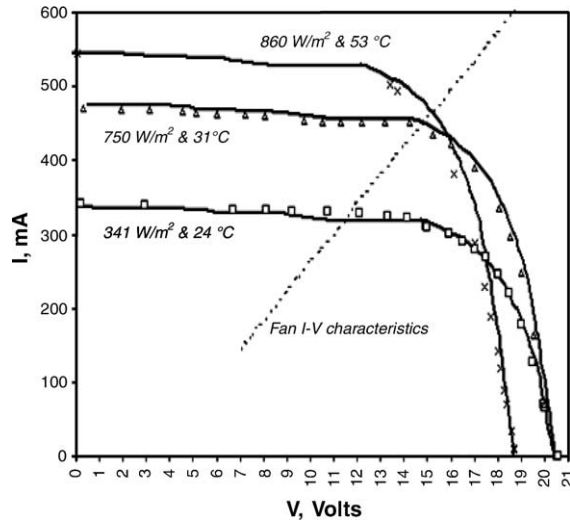


Fig. 2. A comparison of measured and predicted (according to the SANDSTROM model) PV $I-V$ characteristics at different irradiances (W/m^2) and module temperatures ($^{\circ}C$).

Table 1
Data for the two 24 VDC axial flow fans tested

| | Fan1 | Fan2 |
|---|-------------------|--------------------|
| Rated power, W^a | 9.5 | 20.3 |
| Free flow capacity, l/s^a | 69 | 111 |
| Maximum speed (ω_{max}), r/min^a | 2800 | 3500 |
| Maximum pressure at ω_{max} , Pa^a | 93 | 199 |
| $I-V$ characteristic slope, A/V^b | 0.014 ± 0.003 | 0.032 ± 0.005 |
| $\omega-V$ characteristic slope, $r/V \min^b$ | 108.8 ± 1.6 | 125.3 ± 2.2 |
| A , $Pa \ s^3/l^b$ | $-1.1e-3 \pm 0.0$ | $-7.0e-4 \pm 0.0$ |
| B , $Pa \ s^2/l^b$ | $8.1e-2 \pm 0.02$ | $6.6e-2 \pm 0.006$ |
| C , $Pa \ s/l^b$ | -2.4 ± 1.0 | -2.6 ± 0.4 |
| D , Pa^b | 47.6 ± 12.5 | 62.4 ± 6.6 |

^a Manufacturer’s data.

^b Measured.

and speed were recorded. The speed of the fan was measured using a DT2236 handheld optical tachometer with an accuracy of $\pm 0.05\%$. The coefficients of determination for the best fit lines ($y = C \cdot x$) were 0.96 to 0.99 for the $I-V$ characteristics and 0.94 to 0.96 for the $\omega-V$ characteristics.

The $I-V$ characteristic (dashed line in Fig. 2) is solved simultaneously with the PV module’s $I-V$ curve to obtain the operational voltage of the fan, while the $\omega-V$ characteristic is used to determine the fan rotational speed (ω , r/min). It is customary to determine the speed of the fan by solving the PV $I-V$ characteristic with the motor equations [19]. Alternatively, bearing in mind that they are valid for a constant torque (i.e. constant pressure across the fan), the $I-V$ and $\omega-V$ characteristics of the fan can be used [14,20]. This is discussed in detail in Section 3.4.

3.2.2. The pressure–flow characteristic (ΔP_f – Q)

The ΔP_f – Q flow characteristic changes with fan speed [15,16] and air density. By measuring a reference curve at known conditions of speed and air density, the ΔP_f – Q characteristic at any other condition can be derived using fan affinity laws [11].

3.2.2.1. Measurements. Reference ΔP_f – Q curves were taken for the fans given in Table 1 at 2000 r/min. Fan ΔP_f – Q characteristics were measured according to ASHRAE procedures [21]. Pressure measurements were performed with an error of ± 0.5 Pa using an Airflow Developments inclined manometer and two pitot static tubes across the fan. Flow rate measurements were performed at the centre of the duct with an error of ± 4 l/s using a self calibrating ultrasonic anemometer with digital LCD display (Anemosonic UA6). Flow rate measurements were based on 2 min averages of 5 s measurements. An average value of flow rate was determined by multiplying the measured flow rates by a factor of 0.9. This procedure, which substitutes for a full traverse of the duct, can cause an inaccuracy of 5–10% [22].

The speed of the fan was measured using the aforementioned optical tachometer, while the air temperature was measured to ± 0.1 °C using a k -type thermocouple. Rotational speed and air temperature were recorded for each pressure–flow measurement to check their stability.

3.2.2.2. Results. The reference ΔP – Q curve (i.e. 2000 ± 25 r/min (209.4 ± 2.6 rad/s), 18 ± 0.1 °C and 758 ± 0.5 mmHg) for Fan2 is compared to manufacturer’s data in Fig. 3.

Measurements were not obtainable at low static pressures and high flow rates because of the resistance to flow caused by the measuring instrument. The curve shown is typical for axial flow fans [11]. The “dip” in the measured curve is due to the stall conditions on the blade aerofoils.

The ΔP_f – Q characteristic at reference conditions was approximated by a cubic regression with an R^2 value of 0.9844 (for Fan2) and 0.9911 (for Fan1). The ΔP_f – Q characteristics at other conditions are obtained from these cubic regressions as explained below.

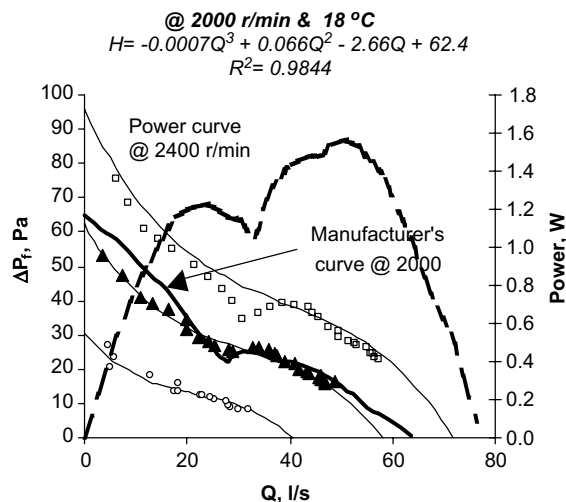


Fig. 3. Fan performance curves (ΔP_f – Q) for Fan2: a comparison of measured (the points) and predicted curves (the solid lines) at three fan speeds (from lower to higher curve: 1400, 2000 and 2400 r/min).

The speed of the fan is obtained as discussed in Section 3.2.1. For a given atmospheric pressure (P_{atm} , mmHg), air temperature (T_{air} , °C) and fan speed (ω , r/min), the flow rate of air at new conditions (Q , l/s) and the corresponding pressure across the fan (ΔP_f , Pa) can be obtained from the reference flow rate (Q_{ref} , l/s) using the following equations:

$$Q = \left[1.92 \times 10^{-4} \frac{\omega \cdot P_{atm}}{T_{air} + 273.15} \right] \cdot Q_{ref} \tag{6}$$

$$\Delta P_f = 3.67 \times 10^{-8} \frac{\omega^2 \cdot P_{atm}^2}{(T_{air} + 273.15)^2} (A \cdot Q_{ref}^3 + B \cdot Q_{ref}^2 + C \cdot Q_{ref} + D) \tag{7}$$

The constants A through D and the experimental errors associated with them are shown in Table 1 for each of the fans. These constants are fan specific and are obtained from the reference regression curve (see Fig. 3). Accounting for all experimental sources of error, the flow rate and pressure in Eqs. (6) and (7) are predicted with errors of 5% and 8%, respectively.

Using Eqs. (6) and (7), ΔP_f – Q curves at 2400 r/min and 1400 r/min were generated as shown by the dark solid curves in Fig. 3. Furthermore, data were measured for Fan2 at 2400 r/min and 1400 r/min and compared to predictions as shown in Fig. 3. Even though a considerable agreement is observed between the predicted and measured values, the cubic regression does not account for the dip in the curve. An alternative way for representing the fan ΔP_f – Q characteristic is to describe it in terms of three linear segments [8].

Fig. 3 also shows the pneumatic power characteristic for Fan2 at 2400 r/min. It is seen that the highest pneumatic power ($\Delta P_f \cdot Q$) is obtained at the top of the lower section of the ΔP_f – Q curve [23]. An optimal length of duct can be determined so that the system operates at that power.

3.3. Duct model

The system ΔP_s – Q curve is a quadratic function of ΔP_s in Q

$$\Delta P_s = K \cdot Q^2 \tag{8}$$

where the coefficient K is a function of the duct properties and density of air as shown in the following equation, which can be derived from Darcy’s law

$$K = \frac{8f \cdot \rho \cdot L}{\pi^2 \cdot D^5} \tag{9}$$

where the friction factor, f , is a function of Reynolds number ($\frac{4\rho \cdot Q}{\pi \mu D}$) and the roughness of the duct (k , mm) and can be obtained from the following equation [24]

$$f = \frac{1.325}{\left(\ln \left(\frac{k/D}{3.7} \right) + \frac{5.74}{N_{Re}^{0.9}} \right)^2} \tag{10}$$

For a flexible duct, the roughness is a function of the degree of extension (or compression). Thus, the ΔP_s – Q curve depends on the degree of extension of the duct in addition to its diameter and length. From the equations above, it is seen that if the roughness coefficient is known for a given extension, the task of determining the system curve for any length and diameter of duct becomes simple.

Abushakra et al. [25] introduced a pressure drop correction factor (*PDCF*) for flexible ducts as a linear function of compression ratio. This factor is defined as the ratio between two pressure drops for two different extensions of the same length of duct. This method, however, is only useful for pressure loss determination and not for generating the ΔP_s – Q curve at a given extension. In the current study, pressure–flow measurements were taken for two duct extensions (80% and 100%) of known lengths and diameters at room temperature. Eqs. (8)–(10) were then used to calculate an average value of roughness (k) for each extension.

The duct used was 3 m long and 152 mm in diameter Thermaflex Aliflex flexible ducting with multiple layer aluminium/polyester laminate. Using these measurements and the equations above, a roughness value of 2.5 ± 1.2 mm is obtained for 100% extension and 9.6 ± 1.5 mm for 80% extension. Values of 2.1 mm for fully extended and 6.3 mm (i.e. 3 times the value at 100% extension) for 80% extended metallic ducts are given by ASHRAE [26].

These experimentally determined roughness coefficients can then be used in Eqs. (10), (9) and (8), respectively, to generate the system curve for any length of duct if the extension, air properties (i.e. air density and viscosity) and duct diameter are specified. Considering all experimental sources of error, the pressure (ΔP_s) in Eq. (8) can be predicted with an error of ± 0.5 –3 Pa (for 80% Ext.) depending on the flow rate, duct length and duct diameter. Fig. 4 shows a comparison of predicted (based on the predetermined k values) and measured ΔP_s – Q curves for a duct diameter of 152 mm and a temperature of 20 °C.

3.4. The effect of pressure on fan characteristics

The “slate packing” affects the system ΔP – Q characteristic. Thus, the flow rate–irradiance (Q – G) profiles are different for different slate types even if the same PV –fan–duct combination

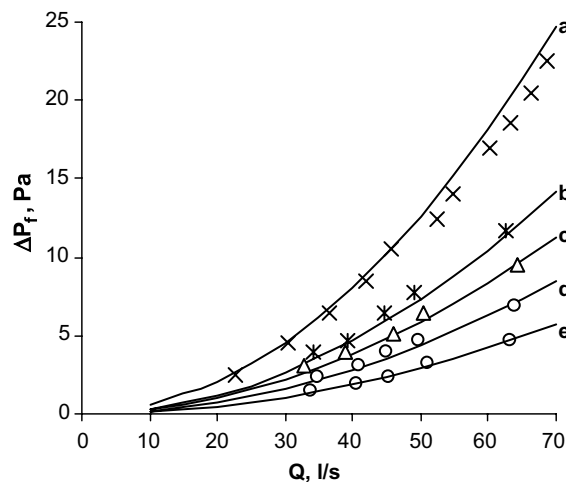


Fig. 4. System performance curves (ΔP_s – Q): a comparison of measured (the points) and predicted curves (solid lines) at 20 °C for different lengths and extensions (a) $L = 5$ m, Ext. = 80%, (b) $L = 5$ m, Ext. = 100%, (c) $L = 4$ m, Ext. = 80%, (d) $L = 3$ m, Ext. = 80% and (e) $L = 2$ m, Ext. = 80%.

is used. Moreover, it is reported that for pumping systems, the fan $I-V$ and $\omega-V$ linear relationships mentioned in Section 3.2.1 change as the pressure across the pump changes [14]. This leads to the conclusion that the speed of the fan and consequently its $\Delta P-Q$ characteristic may also be affected by the “slate packing”, thus affecting the flow rate.

The effect of pressure on the $I-V$ and $\omega-V$ characteristics of fans was experimentally investigated in a 2.5 m long, 141 mm diameter steel tube with the fan at one end of the tube and a restriction valve at the other. Opening and closing the valve alters the pressure across the fan. Fixing the pressure at a desired value and varying the voltage (using a power supply), readings of current and speed for different voltages are obtained. However, as the voltage is increased, the pressure in the system also increases. By adjusting the valve position every time the voltage was increased, the pressure across the fan was maintained nearly constant. $I-V$ and $\omega-V$ curves were obtained for different pressures across the fan. The results of the $\omega-V$ curves for Fan2 are shown in Fig. 5.

It is seen that even though pressure is expected to affect the speed, voltage and current individually, it has a negligible effect on the $\omega-V$ and $I-V$ characteristics of the fan. This effect is more significant in pumping systems because of the associated higher system pressures (meters of water rather than centimetres). The model can, thus, be simplified by neglecting the pressure dependence of the $I-V$ and $\omega-V$ characteristics. The following section outlines the computer model for predicting the flow rate of air in the system.

3.5. The computer model

A detailed flow chart of the model is shown in Fig. 6. Reference conditions, which can be either obtained from manufacturer’s data or from measurements on the components, as described in

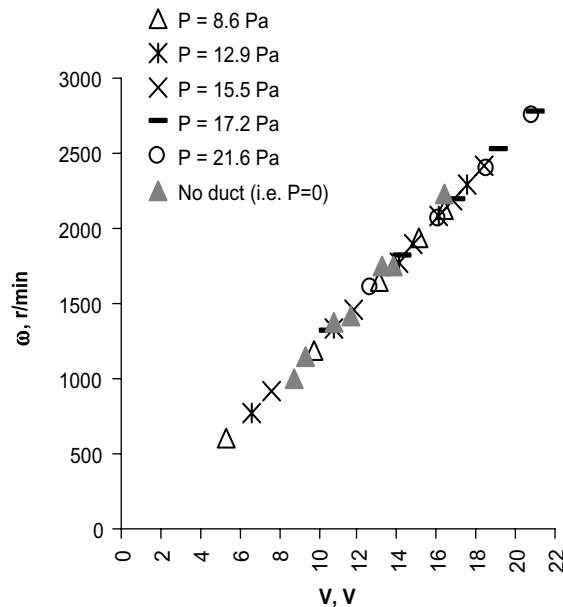


Fig. 5. $\omega-V$ characteristic of Fan2 at different system pressures.

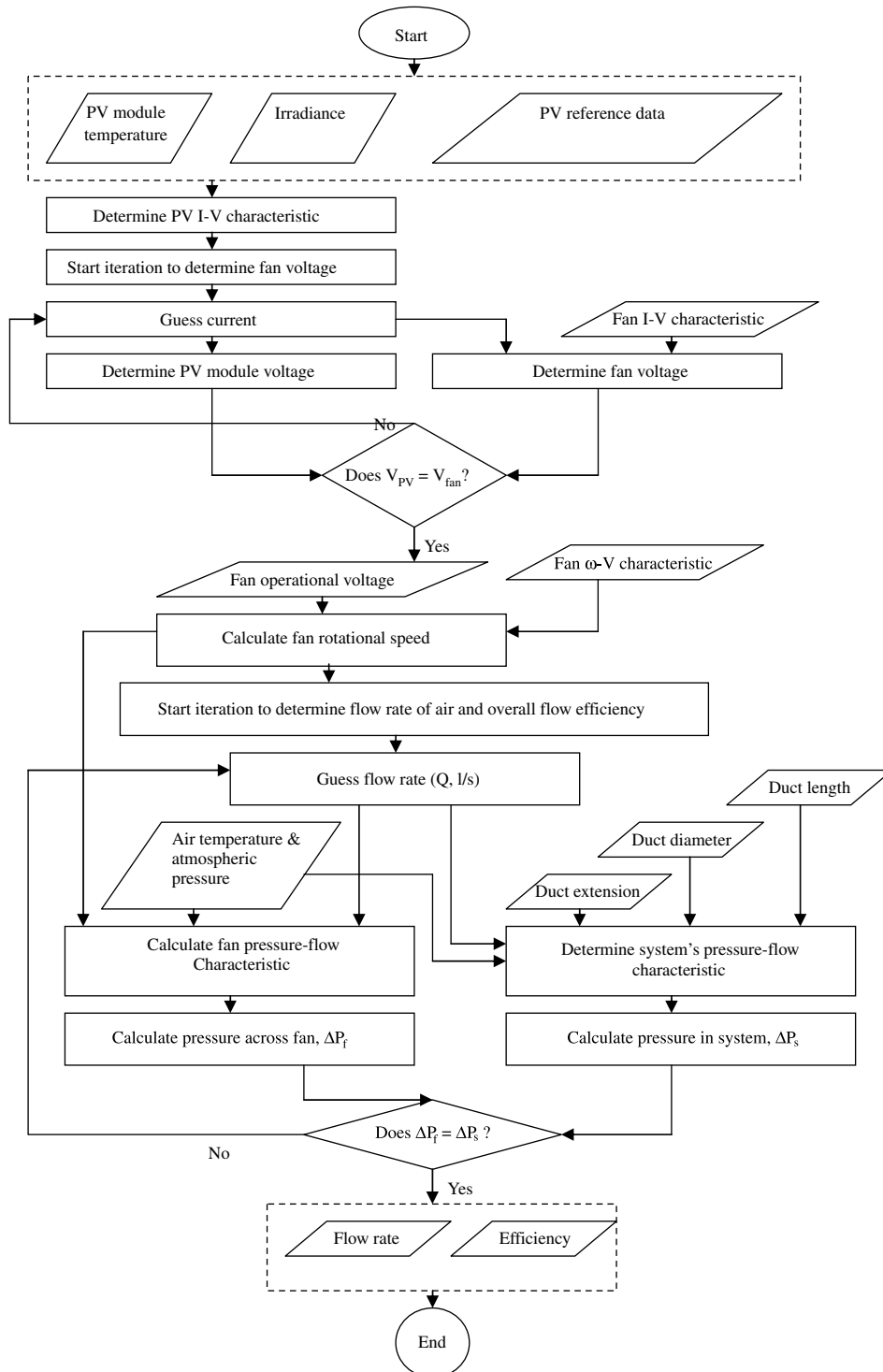


Fig. 6. A detailed flow chart of the computer model.

Sections 3.1–3.3, are necessary for completion of the model. From the irradiance and ambient temperature, the model predicts the PV module's electrical output, which, when solved simultaneously with the fan's electrical characteristic, calculates the rotational speed of the fan. The $\Delta P-Q$ characteristic of the fan is determined at this calculated speed, while that of the fan-duct system as a whole is evaluated with the given duct properties (length, diameter and degree of extension). The flow rate in the system is determined by solving the fan and system $\Delta P-Q$ characteristics simultaneously.

Using the equations above and the experimentally determined reference measurements, a program was written in Visual Basic for Applications (VBA) to calculate the flow rate of air. The model was validated through comparison with measurements as shown in Section 4.

Since the component specific constants used in the model are determined experimentally, the predicted flow rate is expected to have some error. Sources of error include the determination of the PV module reference curve, the coefficients in the fan $I-V$, $\omega-V$ and $\Delta P-Q$ characteristics and the roughness coefficient of the duct. Considering all sources of error in the measurements, the model predicts the rotational speed of the fan and the flow rate with maximum errors of 6.8% and 12.0%, respectively.

4. Model validation

Validation of the program was performed by comparing the predicted performance with that measured for a roof section constructed at the School of Engineering at Napier University in Edinburgh. Predicted flow rates were based on measured values of irradiance, PV module temperatures and in-duct air temperatures.

The roof section shown in Fig. 7(a) was constructed from interlocking concrete tiles. Holes of 10 cm diameter were drilled in the sarking board underneath the slates (Fig. 7(b)) and a well sealed fan box was constructed as shown in Fig. 7(b) and (c). The fan-duct system was installed in the box (Fig. 7(c)) and connected to an MSX-10 Lite BP Solarex PV module, rated at 10 W_p.

Measurements of G , T_{mod} , T_{air} and Q were taken for periods of constant irradiance to ensure stability of flow rate readings corresponding to that irradiance.

The irradiance was measured with an accuracy of 3% [27] using a Kipp and Zonen pyranometer placed in the same plane with the PV module and roof tiles and directly connected to a data logger. Incidence angles were calculated (Azimuth: -15° , Tilt: 45° , Latitude: 55.95° , Longitude: 3.3°) for the time and date of measurement and, whenever necessary, a transmittance correction for irradiance falling on the PV module was applied [28].

Two k -type thermocouples, one placed in the middle at the back of the PV module and the other placed at the outlet of the duct, were used for temperature measurements with an accuracy of $\pm 0.1^\circ\text{C}$. The thermocouples were connected to the data logger, and irradiance and temperature readings were obtained at the beginning and at the end of each flow rate measurement to ascertain the stability of the temperature throughout the measurement period.

Flow rate measurements were performed using the aforementioned anemometer (Section 3.2.2.1) at the centre outlet of the duct as shown in Fig. 7(d).

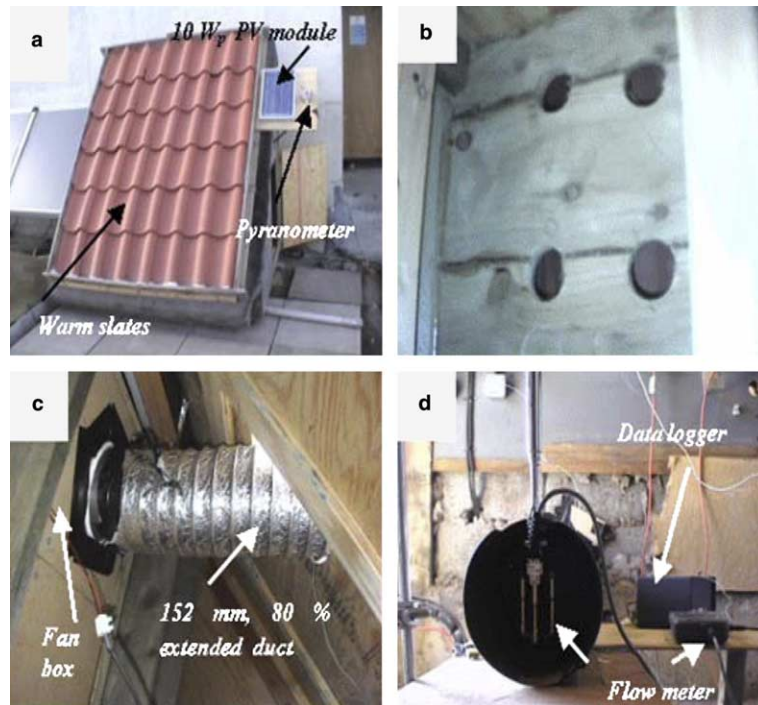


Fig. 7. Tested roof section: (a) roof section, PV module and solarimeter all placed in the same plane, (b) 10-cm holes drilled in the sarking board, (c) the fan and duct at the outlet of the fan box, (d) the flow rate is measured at the duct outlet.

In practise, the duct is not uniformly extended down the attic. If a system curve, ΔP_s-Q is measured in the roof section under investigation then an effective duct length (L_{eff}) can be defined as the horizontal length of duct (at a given % extension and the same duct diameter) that has the same ΔP_s-Q curve as the measured one. For validation purposes, two duct lengths were tested. ΔP_s-Q curves were measured in the roof section and translated into L_{eff} for a 152 mm diameter duct at 80% extension.

In order to measure the system curves, the pressure across the fan, the pressure in the fan box and the flow rate were recorded at different fan speeds (i.e. fan voltages). Pressure measurements were performed with an accuracy of ± 0.5 Pa using the Airflow Developments inclined manometer mentioned above (Section 3.2.2.1) and two pitot static tubes: one placed in the fan box (through a side hole in the joist) and the other downstream from the fan, far enough for pressure recovery to be achieved. The voltage and speed of the fan were manually altered using a Weir 4000 power supply.

The two fans mentioned above (Section 3.2.2) and two effective duct lengths (11.5 ± 1.5 and 8.5 ± 2 m) were tested interchangeably. The results are shown in Fig. 8. The solid line with a slope of 0.9873 and a coefficient of determination of 0.9417 represents the best fit line for all the data points.

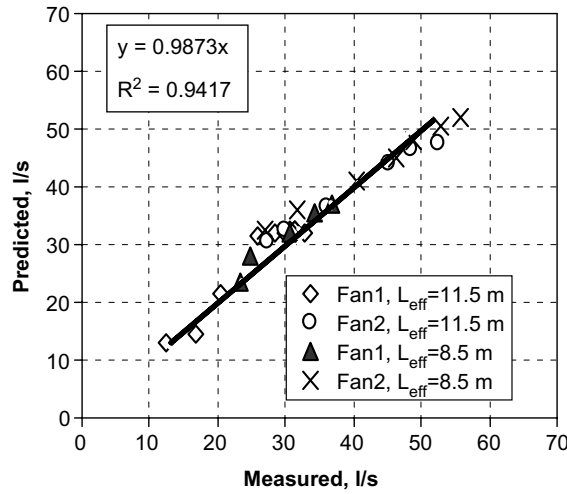


Fig. 8. Predicted vs. measured flow rates for the four systems tested.

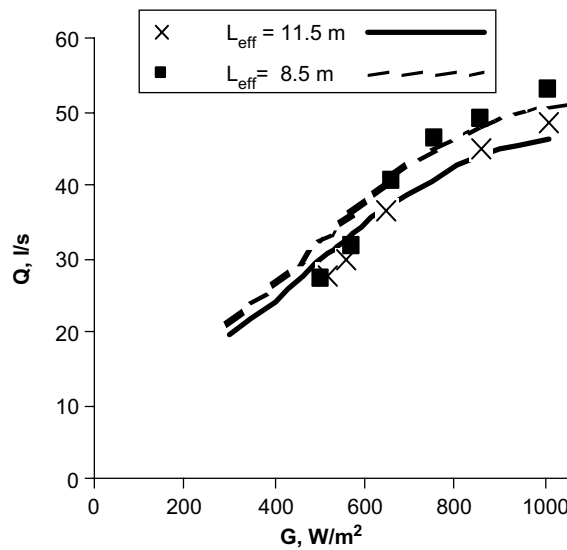


Fig. 9. Predicted (solid lines) and measured Q – G profiles for Fan1 at two effective duct lengths.

For comparison purposes, each of Figs. 9–12 shows a flow rate vs. irradiance (Q – G) profile for two of the four systems. Considering the experimental sources of error inherited by the model and those attached to the measured flow rate, there is good agreement between the measurements and predicted values.

As is seen from Figs. 9 and 10, more flow rate is produced with a shorter length of duct. This is expected because for shorter lengths, the system is working against less resistance to flow.

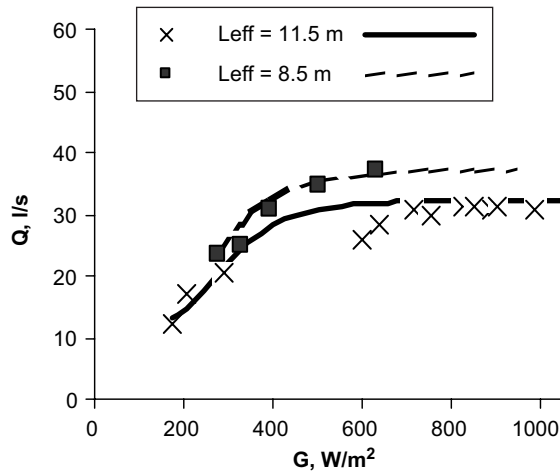


Fig. 10. Predicted (solid lines) and measured Q - G profiles for Fan2 at two effective duct lengths.

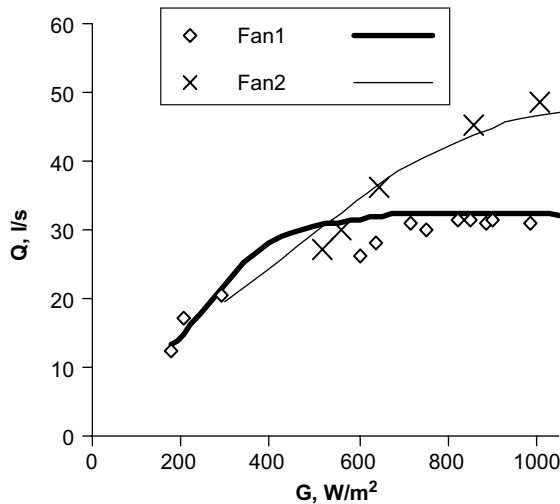


Fig. 11. Predicted (solid lines) and measured Q - G profiles for an effective duct length of 11.5 ± 1.5 m for both fans.

In Figs. 11 and 12, both predictions and measurements reveal that Fan2 provides a lower flow rate than Fan1 at low irradiances but starts producing higher flow rates at some inflection irradiance ($G = 580$ W/m² for the 11.5 m length and $G = 520$ W/m² for the 8.5 m length). For ventilation as well as heating purposes, it is desired to maximise the monthly volume of air delivered (i.e. maximise the flow rate). Thus, it can be concluded from Figs. 11 and 12 that if the monthly averaged irradiance for a certain location is below the inflection irradiance, then it is preferable to use Fan1. Fan 2, on the other hand, is preferable at lower latitudes with higher monthly average irradiances.

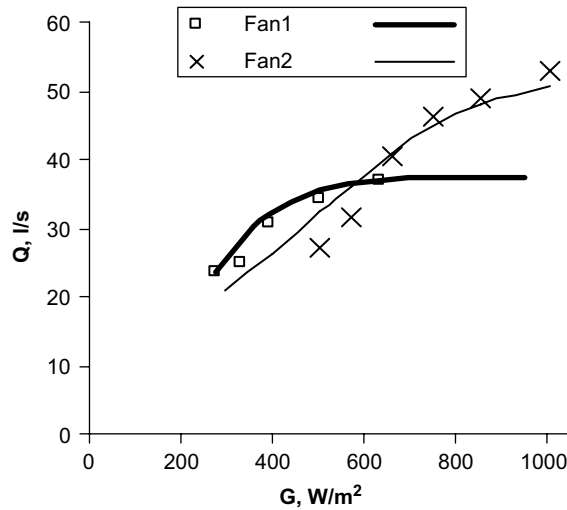


Fig. 12. Predicted (solid lines) and measured Q - G profiles for an effective duct length of 8.5 ± 2 m for both fans.

5. Conclusions

1. Condensation dampness and mould growth are major problems in energy efficient buildings due to the lack of ventilation. A PV driven mechanical (i.e. fan-duct) system, which utilises the solar energy absorbed by the roof slates for preheating ventilation air, is being investigated at Napier University. Understanding the long term performance of this solar ventilation air preheating system requires the development of a model that predicts the flow rate of air as a function of the irradiance falling on the PV module in addition to other factors such as ambient temperature and component (i.e. PV module, fan, duct) specifications.
2. A model has been developed to predict the flow rate of air in the system through consideration of reference measurements. Considering the different sources of experimental error, the model can predict flow rate to $\pm 12\%$. The model has been validated in a roof section at Napier University in Edinburgh for four systems. The predicted values are within 10% of measurements.
3. Even though the roof slates impose a resistance to flow, thus increasing the fan torque and reducing its rotational speed, they have a negligible effect on the fan I - V and ω - V characteristics.
4. For the model developed herein to be applied, the effective length of duct for a given system must be determined. This can be done by measuring the ΔP_s - Q curve in the roof section, and an effective length of duct is determined for a given extension (say 80%). A single measurement of pressure and flow rate is satisfactory to define the ΔP_s - Q curve.
5. The model is extended so that it can be applied for any location (latitude, longitude and weather data of irradiance and ambient temperature) and roof orientation (tilt and azimuth). Future work will make use of the model to optimise the system based on maximising the

monthly volume of ventilation air delivered. The thermal contribution and effectiveness of PV driven RSB systems will also be investigated.

References

- [1] BRE Digest 297. Surface condensation and mould growth in traditionally built dwellings. England: BRE; 1985.
- [2] Gan G, Riffat SB. A numerical study of solar chimney for natural ventilation of buildings with heat recovery. *Appl Therm Eng* 1998;18:1171–87.
- [3] Dai YJ, Sumanth K, Wang RZ, Li YG. Enhancement of natural ventilation in a solar house with a solar chimney and a solid adsorption cooling cavity. *Sol Energy* 2003;74:65–75.
- [4] Khedari J, Ingkawanich S, Waewsak J, Hirunlabh J. A PV system enhanced the performance of roof solar collectors. *Build Environ* 2002;37:1317–20.
- [5] The Nuaire Group. Home ventilation. Drimaster. Caerphilly, United Kingdom, 2004. See also: www.nuaire.co.uk.
- [6] Muhic S, Butala V. The influence of indoor environment in office buildings on their occupants: expected-unexpected. *Build Environ* 2004;39:289–96.
- [7] The Scottish Solar Energy Group. Solar ventilation, examples: Burdiehouse, Edinburgh. Edinburgh, United Kingdom; 2001. See also: <http://www.sseg.org.uk/>.
- [8] Henderson D, Odeh N, Muneer T, Grassie T. Estimating the performance of a PV driven fan in a solar air heating system. In: Deutsche Gesellschaft für Sonnenenergie, PSE GmbH, editors. Proceedings of the 14th EuroSun 2004 International Sonnenforum, 24–26 June, Freiburg, Germany, vol. 1. Freiburg: PSE GmbH; 2004. p. 518–26.
- [9] Letan R, Dubovsky V, Ziskind G. Passive ventilation and heating by natural convection in a multi-storey building. *Build Environ* 2003;38:197–208.
- [10] Al-Ibrahim AM, Klein SA, Mitchell JW, Beckman WA. An investigation of photovoltaic powered pumps in direct solar domestic hot water systems. In: Campbell-Howe R, Wilkins-Crowder B, editors. Proc of Solar '96, American Solar Energy Society, 13–18 April, Asheville, North Carolina, America, 1996. p. 141–6.
- [11] Osborne WC. Fans. 2nd ed. Oxford: Pergamon; 1977.
- [12] Jafar M. A model for small-scale photovoltaic solar water pumping. *Renew Energy* 2000;19:85–90.
- [13] Bione J, Vilela OC, Fraidenraich N. Comparison of the performance of PV water pumping systems driven by fixed, tracking and V-trough generators. *Sol Energy* 2004;76:703–11.
- [14] Hadj Arab A, Chenlo F, Benghanem B. Loss-of-load probability of photovoltaic water pumping systems. *Sol Energy* 2004;76:713–23.
- [15] Betka A, Moussi A. Performance optimization of a photovoltaic induction motor pumping system. *Renew Energy* 2004;29(14):2167–81.
- [16] Eckstein J, Townsend T, Beckman WA, Duffie JA. Photovoltaic powered energy systems. In: Proceedings of the American Solar Energy Society, Austin, Texas, 1990. p. 199–204.
- [17] Benlarbi K, Mokrani L, Nait-Said MS. A fuzzy global efficiency optimisation of a photovoltaic water pumping system. *Sol Energy* 2004;77:203–16.
- [18] Buresch M. Photovoltaic energy systems—design and installation. London: McGraw-Hill; 1983.
- [19] Anis WR, Metwally HMB. Dynamic performance of a directly coupled PV pumping system. *Sol Energy* 1994;53:369–77.
- [20] Cromer C. Sizing and matching a photovoltaic circulation system with a solar domestic hot water system, FSEC-PF-29-83. Florida Solar Energy Center, Cocoa, Florida, 1983.
- [21] ASHRAE. ASHRAE Handbook of Equipment. American Society of Heating Refrigerating and Air Conditioning Engineers, Atlanta, 1988.
- [22] Perry RH, Green DW. Perry's chemical engineers' handbook. 7th ed. New York: McGraw-Hill; 1997.
- [23] Meyer CJ, Kroger DG. Plenum chamber flow losses in forced draught air-cooled heat exchangers. *Appl Therm Eng* 1998;18:875–93.
- [24] Muneer T, Kubie J, Grassie T. Heat transfer—a problem solving approach. London: Taylor & Francis; 2003.

- [25] Abushakra B, Walker IS, Sherman MH. A study of pressure losses in residential air distribution systems. In: Proceedings of the 2002 ACEEE Summer Study on Energy Efficiency in Buildings. Washington, DC: American Council for an Energy Efficient Economy; 2002.
- [26] ASHRAE. ASHRAE 2001 Handbook of fundamentals. American Society of Heating Refrigerating and Air Conditioning Engineers, Atlanta, 2001.
- [27] Kipp, Zonen Incorporated. Kipp & Zonen Instruction Manual, CM3 Pyranometer. Delft, Holland, 2004.
- [28] Duffie JA, Beckman WA. Solar engineering of thermal processes. 2nd ed. New York: Wiley Interscience; 1991.